© 2019. MANUSCRIPT SUBMITTED TO JOURNAL OF EXPERIMENTAL BIOLOGY (2019) 00, jebxxxxxx. doi:10.1242/jeb.xxxxxx

RESEARCH ARTICLE

A gene regulatory network that can adjust developmental timing to in vivo and in vitro cell differentiation dynamics.

Timothy Fulton[1], Kay Spiess[1,2], Lewis Thomson[1], Yuxuan Wang[1], Bethan Clark[1,3], Seong-won Hwang[1], Brooks Paige[2,4], Berta Verd[1,5*] and Ben Steventon[1*]

ABSTRACT

As tissues elongate, cell rearrangement alters positional information as cells move within a morphogen gradient. Despite being present in many patterning systems, the role of cell movements is often ignored. Paraxial mesoderm elongation is an ideal system to study this as cells rapidly mix within the posterior progenitor zone while being exposed to both FGF and Wnt morphogen gradients. By reverse-engineering gene regulatory networks that predict single cell expression trajectories across the tissue, we find a network capable of recapitulating the full range of dynamic differentiation profiles observed both *in vivo* and *in vitro*. Simulating gene expression profiles on *in toto* cell tracking data sets reveal that this gene regulatory network is sufficient to maintain T-box gene expression patterns in the context of real tissue morphogenesis. The model also recapitulates the generation of heterogeneous tbx6 expression in the posterior progenitor zone that we observe by single cell measurements of gene expression in situ. Taken together, these results demonstrate that gene regulatory networks can provide sufficient dynamic range to adjust to cell rearrangement in vivo, and altered developmental dynamics when cultured in vitro.

KEYWORDS: gene regulatory networks, cell rearrangements, pattern formation

INTRODUCTION

During the elongation of the vertebrate body axis, rates of self-renewal and cell differentiation must be precisely coordinated such that a continual supply of progenitor cells are maintained through embryo elongation (1; 2). This temporal coordination is especially important within the presomitic mesoderm (PSM) as it is segmented into somites at the anterior end of the tissue in a clock-like process (3). While much has been studied regarding the temporal dynamics of somitogenesis, less is known about the mechanisms that coordinate cell fate specification in the tailbud as cells progressively mature into a PSM cell state (4). In zebrafish embryos, this maturation is marked by a transition from tbxta, through to tbx16 and then tbx6 expression (5; 6). At the tissue level, a pattern of gene expression emerges that is robust and aligns with a graded decrease in both Wnt and FGF pathway activity (7; 8). Both morphogens generate a wavefront of positional information that has been shown to determine the dynamics of somitogenesis, together with a Notch dependent clock (9; 10; 11; 12).

While cells are undergoing PSM maturation, they are also undergoing a rapid series of cell rearrangements that are required as a driver of PSM elongation. In chick embryos, it has been shown that random cell rearrangements downstream of FGF signalling result in a coordinated posterior expansion of the tissue along the anterior-posterior axis (13; 14). A similar transition from a liquid-like state of high cell motility in the posterior to a more solid-like state in the anterior has been observed in zebrafish embryos (15; 16) and is linked to an increased amount of cell rearrangement in the posterior progenitor zone (17; 18). Analysis of cell rearrangements in 3D further show how cells rapidly exchange neighbours as the tissue compacts in the dorsal-ventral and medial-lateral axes and elongates along the anterior-posterior axis (19). How these movements impact the dynamics of progenitor cell maturation at the single cell level, yet still enable the generation of stable patterns of T-box expression at the tissue level is currently unknown.

Recent work has highlighted the extent to which the dynamics of the zebrafish somitogenesis clock is intrinsic to each cell. Previous studies had shown that cells cultured *in vitro* are capable of eliciting transient oscillations of Notch pathway activity, as assayed with reporters for her1 expression (20). However, it was unclear whether such oscillations might be an emergent property of cell populations operating via local signalling. More recently, it has been demonstrated that her1 oscillations can still be observed within isolated cultures of cells and in the absence of any signals added to the medium (21). Importantly, these cells slow down their oscillations and upregulate mesp expression, a marker of somite polarity (21; 22). These results demonstrate that PSM differentiation is to a large degree cell autonomous in zebrafish embryos. Furthermore, they open the question of how the dynamics of an intrinsic timer can be modulated to match the cell specific dynamics of differentiation that occurs *in vivo* given individual rates of movement from the tailbud.

To investigate the cell-intrinsic mechanisms that time cell differentiation in response to external signalling, a common approach is to reverse engineer a minimal gene regulatory network (GRN) that is sufficient in its description of the system to recapitulate spatial distributions of gene expression observed *in situ* (23). Such

[1]Department of Genetics, University of Cambridge, Cambridge, UK;

[2]The Alan Turing Institute, London, UK;

[3]Department of Zoology, University of Cambridge, Cambridge, UK;

[4]Centre for Artificial Intelligence, University College London, UK;

[5]Department of Biology, University of Oxford, UK

Authors for correspondence: berta.verdfernandez@biology.ox.ac.uk, bjs57@cam.ac.uk

Received 1 April 2023; revised

an approach has been successful increasing our understanding of the dynamics of morphogen interpretation in a range of systems including the *Drosophila* blastoderm and vertebrate spinal cord (24; 25; 26; 27). However, inferring GRNs that can recapitulate the emergence of gene expression patterns in the context of rapid cell rearrangements is challenging. Here, we aim to ascertain whether a single gene regulatory network (GRN) can predict the full dynamics of PSM differentiation in both *in vivo* and *in vitro* contexts.

To determine the range of timings for the movement of cells out of the tailbud, we first probed the limits of their differentiation dynamics by culturing tailbud progenitors *in vitro* and assayed the proportion of tbx16/6 expressing cells at subsequent timepoints. We then compared this to *in vivo* where cells undergo a range of differentiation dynamics as a function of the time spent in the posterior progenitor domain, and so are distributed across a broad range of temporal trajectories. In a companion paper (8), we developed a fitting and modelling framework that can operate in the context of cell movements within the zebrafish PSM through the mapping of gene expression patterns onto *in toto* cell tracking datasets. We first approximated gene expression trajectories (AGETs) in single cells which were then used to reverse engineer the parameters of a three transcription factor, two-signal network (8). Here, we ask whether any of the parameter sets obtained through this approach are sufficient to recapitulate all progenitor maturation dynamics observed both *in vivo* and *in vitro*.

RESULTS.

A cell intrinsic timer drives differentiation of only a subset of tailbud progenitors.

It has been previously reported that when cells are explanted from the PSM of the zebrafish embryo, this triggers an intrinsic timer to differentiate into Mesp positive somitic mesoderm (21). To assay the autonomy of T-box expression changes in isolation, we aimed to measure tbx16 and tbx6 expression changes in single cells explanted from the posterior-most region of the tailbud. To check that we were able to accurately explant the posterior progenitor region, we first injected embryos with nls-KikGR, a photo-covertible protein that is targeted to the nucleus (28). Explants were then taken from injected embryos where the posterior 25% of the tailbud had been photo-labelled (Figure 1A). This confirmed that the posterior-most region (containing cells with low levels of tbx6 expression) was being taken for dissociation and subsequent cell culture (Figure 1A; inset). To confirm the gene expression state of these cells, we stained them for tbx16 and tbx6 and showed that most cells express high levels of tbx16 with only a few cells expressing tbx6 (Figure 1B).

Explants taken from the posterior tailbud were dissociated by gentle agitation in calcium and magnesium free PBS to produce single cells in suspension, and cultured in adherent culture under a media of defined L15 with no serum or signal factor supplementation, as previously described in (21). Under these culture conditions, cells downregulated expression of tbx16 and upregulated their expression of tbx6 over a period of 6 hours, as measured by HCR on fixed timepoint samples imaged at high magnification (Figure 1C). Further examination using a tbx6::GFP reporter (29) revealed that GFP fluorescence increased in only a proportion of cells and that the GFP signal onset began in a proportion of cells after approximately 200 minutes (3.5 hours) in culture (Figure 1D,E).

Cells stained using multiplex HCRs for tbxta, tbx16, tbx6 and keratin18 at each time point were manually classified into five categories: progenitors, which expressed tbxta and/or tbx16, tbx6 positive cells, epidermal cells expressing keratin18, dead cells which showed abnormal nuclei shape or fragmented nuclei, and other. Very few cells are observed dividing over this time course. Over time, the proportion of tbx6 positive cells increases at the expense of cells in the progenitor category (Figure 1F-G). These results together demonstrate that once isolated *in vitro*, cells from the posterior 25% of the tailbud have the potential to mature into tbx6 positive cells and that this starts at approximately 3.5 hours in culture.

Journal of Experimental Biology (2019) 00, jebxxxxxx. doi:10.1242/jeb.xxxxxx

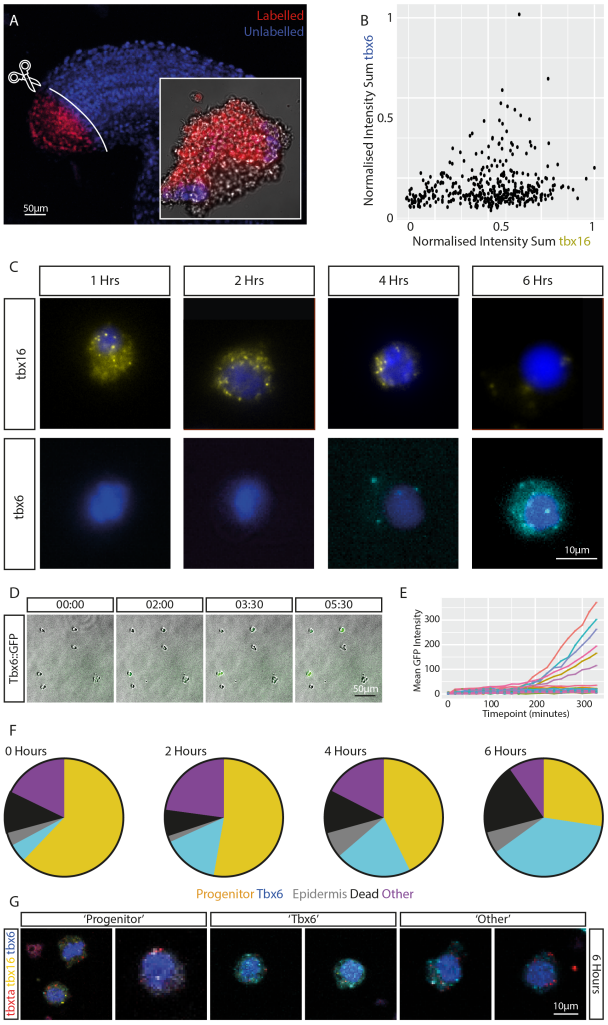

Fig. 1. Presomitic Mesoderm progenitor cells differentiate *in vitro* forming a bimodal population of cells. (A) Labelling and dissection of the posterior 25% of a 21 somite stage tailbud demonstrates explants are produced mostly of labelled cells. Explant shown in image insert. **(B)** From HCR data on whole explants, it is demonstrated that they are made of cells expressing tbx16 and only a small number of tbx6 expressing cells. By dissociation of these cells into single cells and culturing them in L15 media without supplementation **(C)** cells are observed downregulating expression of tbx16 and increasing expression of tbx6 in fixed time points using HCR. **(D)** Using live imaging of a tbx6::GFP reporter, it was observed that GFP is observed only in a proportion of cells and that the **(E)** GFP signal appears synchronously in multiple cells after approximately 200 minutes *in vitro* culture. Cells not expressing GFP at this time do not express GFP even after 300 minutes of culture. Minimal to no cell divisions are observed occurring over the time course. **(F)** Through manual classification of single cell multiple HCR using tbxta, tbx16, tbx6, keratin18 probes, cells were defined as: "progenitor" (expressing tbxta and tbx16), "tbx6" (expressing tbx6), "Epidermis" (expressing keratin18), "Dead" (with fragmented or unusual nuclei) or "Other" (none of the above gene expression patterns). It was observed the majority of cells begin the culture period as progenitors and that this proportion decreases as the proportion of tbx6 cells increases. The proportion of epidermis, other and dead cells stays relatively stable with some increase in dead cells by six hours. **G** Examples of Progenitor Cells, tbx6 cells and cells classified as Other which express both tbxta and tbx6 together at the six hour time point. **(C)** n = 3 biological replicates; images representative. **(F)** Displayed data from single experiment containing: 0hrs n=140 cells, 2hrs n=123 cells, 4hrs n= 143 cells, 6hrs n=186 cells

Cells *in vivo* differentiate over a range of time-scales.

We next aimed to relate the dynamics of T-box gene expression observed *in vitro* to the range of differentiation trajectories cells undertake *in vivo*. We first measured the time taken for a clone of 15-20 photo-labelled cells to spread from the from a tbxta positive progenitor region (Figure 2A) into a newly made somite (Figure 2C). Embryos were injected at the 1-cell stage with mRNA encoding a mRNA encoding nls-kikGR, and then photo-labelled in the posterior progenitor region at the 21 somite stage. We observed that in multiple embryos, the fastest cell entered a somite within 3 hours of being labelled in the posterior, with other cells exhibiting a range of longer times depending on how long they took to exit the progenitor domain. This streaming behaviour of the photo-labels placed in the progenitor domain is in contrast to the coherent distribution of clones observed when cells are labelled in the PSM (19), and is consistent with the idea that the non-directional movement of cells in the progenitor zone helps to generate a progressive entry of cells into the posterior PSM.

To relate these cell movements to transitions in T-box gene expression, we used HCR to stain for tbtxa, tbx16 and tbx6 mRNA (Figure 2D-G). We masked the notochord and notochord progenitor cells and removed this tbxta signal from the image so that only the tbxta expressed within the PSM remained (Figure 2H-K). The intensity of the HCR signal was then plotted across the PSM, normalizing the axis (where 0 represents the posterior end of the tailbud and 1, the posterior-most boundary of the most recently formed somite) (Figure 2I,J). This made it possible to quantify the expression patterns of the three T-box genes across the presomitic mesoderm and tailbud (Figure 2H-J). Our analysis revealed that cells undergo a range of temporal trajectories in gene expression, with the fastest cells transiting through to a newly formed somite in 3 hours.

Journal of Experimental Biology (2019) 00, jebxxxxxx. doi:10.1242/jeb.xxxxxx

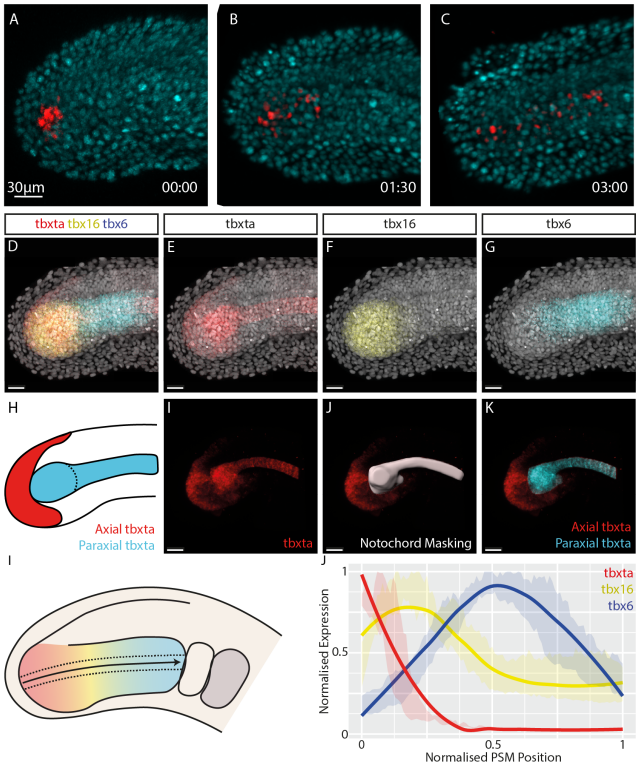

Fig. 2. Stable patterns of T-box gene expression are formed across the presomitic mesoderm and tailbud despite cell mixing. (A-C) Labeling of the posterior of the presomitic mesoderm in a 21 somite stage embryo demonstrates that cells spread throughout the entire tissue with the fastest cell entering the newly formed somite in 3 hours whereas other cells differentiate over a continuous range of timescales. **(D-G)** The T-box gene expression domains within the presomitic mesoderm using HCR against tbxta, tbx16 and tbx6 at the 21 somite stage. Representative images shown. **(H-K)** Axial tbtxa expression was masked in 3D, and ignored during analysis to allow quantification of tbxta expression only within the paraxial mesoderm. An example of the region masked, and the masking process is shown. **(I)** Expression of T-Box genes are quantified by generating a maximum projection of the 3D image, then quantifying expression across a central zone, from posterior to anterior. **(J)** These quantified levels of expression are plotted along a normalized posterior (0) to anterior (1) axis where 1 represents the posterior boundary of the most recently formed somite. Intensity of signal was also normalized between 0 and 1 from multiple embryos plotted together. Ribbon = range of values measured; line = mean.

A reverse-engineered GRN recapitulates tissue-level T-box pattern formation and *in vitro* T-box gene expression dynamics.

We have observed that tailbud progenitors can differentiate over a range of timescales in both *in vitro* and *in vivo* contexts. To investigate the underlying mechanisms that enable this, we set out to reverse-engineer a GRN that could be interrogated in a manner that links intrinsic gene-regulatory dynamics with cell movement. GRNs formulated as dynamical systems have been very helpful elucidating patterning mechanisms (see for example (30; 31; 32) among many others), however existing methodologies to infer GRNs from quantitative gene expression data have bypassed the role of cell movements in patterning processes. For this reason we developed a methodology that would allow us to infer GRNs driving pattern formation in tissues undergoing morphogenesis which explicitly accommodated cell rearrangements and movements and applied it to the developing zebrafish PSM (8).

To reverse-engineer GRNs from our HCR data we first constructed approximated gene expression trajectories (AGETs) that approximate temporal changes in T-box expression and Wnt and FGF signalling as cells move through the PSM. To achieve this we combined a) HCR stains of tbxta, tbx16 and tbx6 expression (Figure 2 D-J), canonical Wnt activity as determined by the activity of a TCF-GFP reporter line (33) (Figure 3A,C), FGF signalling activity through measurements of di-phosphorylated ERF antibody staining (Figure 3B-C), and 3D cell tracking data from time-lapse imaging datasets of the PSM (Figure 3D). In both T-box expression and signalling activity datasets, nuclei of the PSM were segmented and the corresponding intensity values carried forward along with the point cloud (3D spatial) coordinates of each cell. These were aligned with the cell tracking datasets using an iterative closest point algorithm (Figure 3 - Supplementary Figure 1A-B) (8). Once aligned, AGETs are calculated to approximate Tbox and signalling dynamics, and used to infer a GRN model of T-box gene expression (Figure 3 - Supplementary Figure 1C). We used a small randomly spaced subset of 10 AGETs and a Marcov Chain Monte-Carlo algorithm to obtain sets of candidate GRN parameters (Figure 3 - Supplementary Figure 1D).

We next selected and clustered the networks that were able to recapitulate tissue-level T-box patterning when simulated on the tracks, in addition to providing a good fit to the 10 AGETs used for fitting. We simulated GRNs directly onto all the cell tracks obtained from *in toto* live imaging (Figure 3D), by formulating the GRN in each cell and simulating all of these in parallel using quantitative measurements of signal activity as inputs (Figure 3A-C) (we refer to this as live-modelling due to its parallel to live-imaging). This method allows us to observe the emergence and maintenance of pattern at the level of the tissue from the dynamics of gene expression being simulated in the single cells (Figure 3E), while still taking into account cell rearrangements explicitly. We obtained 22 clusters of network. Here, networks were clustered according to their quantitative parameter values, considering the value of parameters in addition to their sign (either an activation or an inhibition (8)). Considering the sign alone results in 15 distinct network topologies that were capable of providing a good fit to each AGET across the anterior-posterior length of the PSM (Figure 3 - Supplementary Figure 2). Note that these networks fail to capture the depletion of tbx6 at the anterior of the PSM as this is known to be due to additional anterior repressors such as Ripply1 (34) that are absent in our model (Figure 3F,G).

Journal of Experimental Biology (2019) 00, jebxxxxxx. doi:10.1242/jeb.xxxxxx

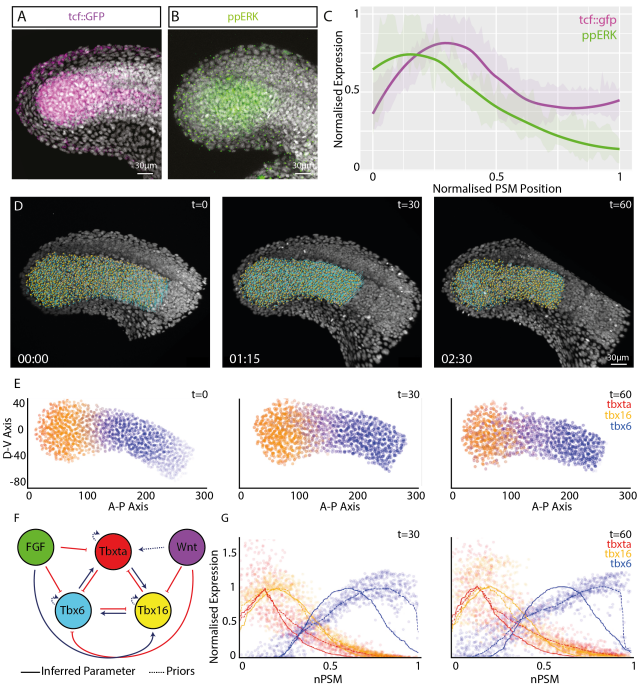

Fig. 3. A Reverse Engineered Gene Regulatory Network Can Recapitulate *in vivo* Patterns of T-box Gene Expression With Cell Movements. A-B Measurements of the signalling environments within the PSM were made by either measuring the level of gfp mRNA produced from a 7XTCF::GFP reporter to measure the level of Wnt signalling, or via an antibody stain against diphosphorylated ERK to measure FGF signalling at the 21 somite stage. **C** These images were quantified along a normalised PSM axis as in Figure 2J. **D** We obtained live imaging data of the developing zebrafish PSM from the 21 somite stage onward and tracked individual cells over 02:30hrs. t=0 shows the first frame in the time lapse where every nucleus in the PSM is highlighted by the tracking algorithm with a spot. t = 30 shows the 30th time frame which corresponds to 01:15hrs into the time-lapse and t = 60 shows the 60th frame in the movie, which corresponds to the end of the time lapse at 02:30hrs. Data from (19). In these tracking data, newly formed somites were deleted as soon as the morphological somite is formed. Non-presomitic mesoderm tracks were deleted from the entire movie at all time points. **(E)** The tracking data in (D) were used to implement the live–modelling framework where reverse-engineered zebrafish T-box GRNs are simulated on every cell track represented *in silico*. The live-modelling framework allows us to observe how tissue-level patterning emerges as a function of GRNs acting at the single cell level as the PSM undergoes morphogenesis. tbxta in red, tbx16 in yellow and tbx6 in blue. **F** Reverse-engineered T-box GRN. **G** Quantified simulated gene expression patterns compared to the gene expression patterns measured in the embryo, previously quantified using HCR. Each dot represents the simulated concentration of a T-box gene in a single cell. Curves (dotted lines) were fitted and normalised to the simulated gene expression and compared to the quantified experimental data (solid lines) at different time points (t=30 and t=60 shown here) to assess the goodness of fit. (A-C) n=6 biological replicates; all data plotted; line represents mean; ribbon represents range.

We next asked whether a single GRN can provide sufficient dynamic range to also recapitulate the gene expression dynamics observed when cells are cultured in vitro. We first quantified signalling dynamics in the *in vitro* experiments, and used these to simulate all 22 representative networks and selected networks that also recapitulated the T-box expression dynamics measured *in vitro* (Figure 3 - Supplementary Figure 1E). To characterise the levels and dynamics of Wnt and FGF signals *in vitro* we quantified Wnt signalling activity by performing HCR against gfp mRNA produced from a Tg(7xTCF-Xla.Siam:GFP) zebrafish reporter line which reports on active Wnt signaling (33) while FGF was assayed using antibody staining against diphosphorylated ERK (Figure 4A-B). Quantification of these signals in multiple cells *in vitro* revealed that the levels of Wnt and FGF signaling decline in single cells over the 6 hours of culture. The cell population maintains high ppERK phosphorylation during the first 4 hours before downregulating it at 6 hours (Figure 4C). Mean TCF reporter levels also decline rapidly within the first two hours of culture and remain low for the remaining duration of the timecourse (Figure 4D). Next, we imaged at the single cell level *in vitro* using HCR stains against tbx16 and tbx6 experiments and quantified expression levels by masking around individual cells normalised by cell area. From this we found bimodal differentiation dynamics in single cells, where a population of cells increased their levels of tbx6 and downregulated tbx16, while at the same time, other cells remain tbx6 negative (Figure 4E,G).

Out of 22 networks, ten recapitulated both the downregulation of tbx16 (Figure 4E,F) and the bimodal activation of tbx6 in single cells in vitro (Figure 4G,H). Unable to discriminate between these further based on fit, we selected a network whose predicted interactions were also supported by the current literature, namely, the network where tbx16 is predicted to activate tbx6. This has been demonstrated in heatshock regulated tbx16 overexpression lines which yield an increased expression of tbx6 (35). Additionally, mutants in tbx16 have a loss of tbx6 expression (36) further evidencing this interaction. It is also known that FGF activates tbx16 expression as dominant negative FGFR1 embryos display a loss of tbx16 expression (37; 38). In imposing this selection criteria, the remaining network proposed also infers that Wnt signalling will repress the expression of tbx6; an interactions which is also supported by experiments that show overexpression of the Wnt inhibitor protein DKK1 results in an expansion of tbx6 expression (36). The experimental evidence that Wnt activates expression of tbxta, as Wnt signalling activity inhibition results in a loss of tbxta expression, has also been incorporated within this model as a non-inferred prior parameter (35; 37). Taken together, these results propose a GRN (Figure 3F) that has a number of inferred and prior known interactions supported by the literature and capable of predicting differentiation dynamics of tailbud progenitors *in vivo*, on cell tracks, and when cultured as single cells *in vitro*.

Journal of Experimental Biology (2019) 00, jebxxxxxx. doi:10.1242/jeb.xxxxxx

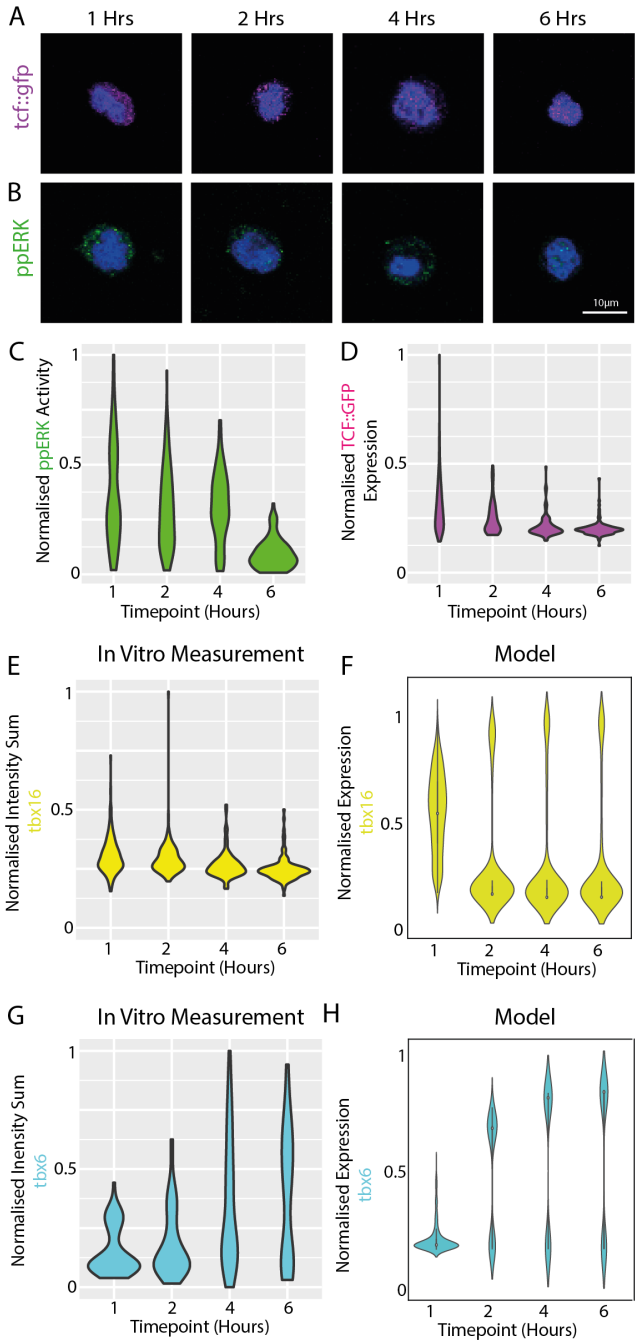

Fig. 4. *In vitro* cultures of PSM cells differentiate as single cells with dynamics predicted by a simulated gene regulatory network. Progenitor cells were taken from a 21 somite stage emberyo and cultured *in vitro*. **(A-B)** Cells maintain some level of Wnt and FGF signalling measured by gfp mRNA production from a 7XTCF::GFP reporter or diphosphorylated ERK antibody staining respectively. Examining these stains at the single cell level demonstrate that **(C-D)** the level of FGF and Wnt signalling declines over the time course with a gradual decline in mean ppERK activity and a more rapid decline of TCF::GFP activity over time. **(E & G)** Examining single cell HCRs for tbx16 and tbx6 demonstrate that the level of tbx16 declines and the level of tbx6 increases in only some cells to form a bimodal population by 6 hours, where some cells are tbx6 positive and others and still low in tbx6 expression. **(F & H)** Using the remaining 22 reverse engineered networks which could generate patterns similar to those observed in vivo when simulated on cell tracking data, simulation of single cells cultured *in vitro* and imaged as individuals also predicted the formation of a bimodal population, as was observed *in vivo*. **(E-H)** n=3 biological replicates; one experiment plotted; data representative.

Cell movement direction, and not total displacement, correlates with tbx6 upregulation in the PSM.

Our live-modelling framework makes it possible to explore the differentiation dynamics of single cells within the PSM and to associate these dynamics with the cells' relative positions and movements. We investigated how cells change their dynamics of T-box expression as a function of their changing position by choosing two cells that both begin the simulation at 23% posterior-anterior position, but that as development proceeds, will diverge in their positions and overall 4D trajectories: one cell will leave the progenitor region and enter the PSM, making its way towards a somite (Figure 5A), while the other will remain in the progenitor region even moving slightly posteriorly over time (Figure 5D).

The first thing to note is that the signalling AGETs and initial Tbox concentrations are not the same for both cells despite them being located at the same antero-posterior position. This reflects the fact that AGETs are constructed from 3D gene expression quantification and retain the heterogeneity present in the data, which is present even across narrow spatial domains (8). The next thing to note, is that the cell that moves anteriorly will continue to upregulate FGF and downregulate Wnt (Figure 5B), while the cell that remains in the progenitor region will maintain high Wnt signalling levels and low FGF (Figure 5E). The cell which exited the progenitor region is predicted by the model to reduce its tbxta and tbx16 expression levels and slowly increase tbx6 expression (Figure 5A,C). By contrast, the cell which remains embedded in the progenitor region throughout the simulation, is predicted to maintain high levels of tbxta and tbx16 expression, and a low level of tbx6 expression (Figure 5D,F). Together, this provides an example of how the live modelling approach can be utilised to explore how individual cell gene expression trajectories might be impacted by cell movement and/or its initial gene expression conditions.

Our model suggests that it is a cell's overall movement along the anterior-posterior axis rather than the total distance it travels (track length) that determines its maturation dynamics. Figure 5G shows that cells starting in the posterior-most 25% region of the progenitor region will experience a larger change in tbx6 expression levels if their overall displacement is positive (towards the anterior) than negative (towards the posterior), as reflected by the larger lightly-coloured area in the top left quadrant as compared to the bottom left one. In contrast, the total distance travelled by a cell in the same region does not correlate with the level of tbx6 change that it will experience, which is shown by the comparable shading in both top and bottom left quadrants in Figure 5H. These observations suggest that cell movements could have a role in modulating the dynamics of progenitor maturation by generating dynamic exposure to spatial signalling environments. However, local heterogeneity in gene expression levels between individual cells is likely to be a key determinant in the rate of gene expression change as this determines the initial conditions for each trajectory simulation.

Journal of Experimental Biology (2019) 00, jebxxxxxx. doi:10.1242/jeb.xxxxxx

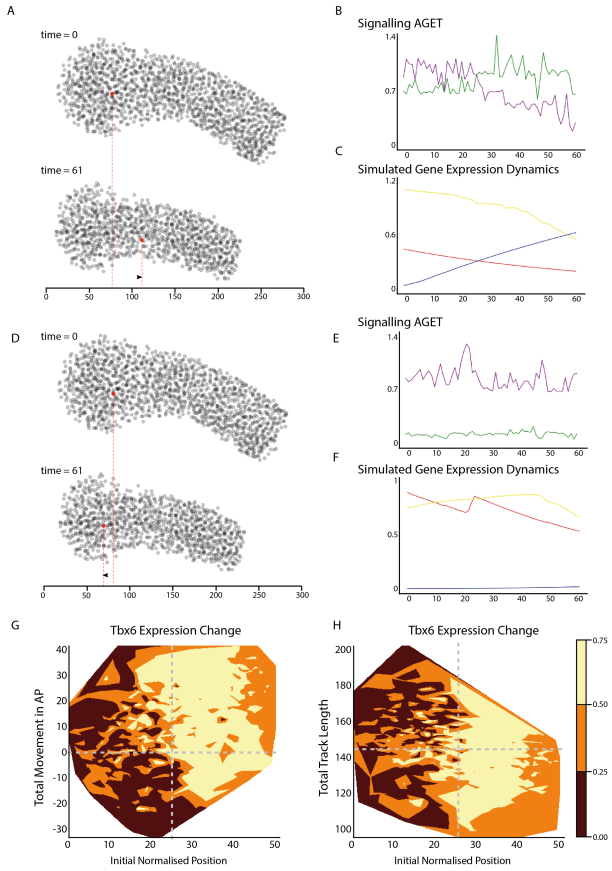

Fig. 5. Tbx6 upregulation is a function of cells' initial position and the total distance travelled along the posterior-to-anterior PSM axis, but not of the total distance travelled. (A. top) Relative position of the cell within the zebrafish PSM at the start of the simulation (23.8321% posterior-anterior at time = 0) and **(A. bottom)** at the end of the simulation (time = 61). **(B)** Signalling AGET and **(C)** simulated T-box gene expression dynamics for the cell shown in (A). **(D. top)** Relative position of the cell within the zebrafish PSM at the start of the simulation (23.8361% posterior-anterior at time = 0) and **(D. bottom)** at the end of the simulation (time = 61). **(E)** Signalling AGET and **(F)** simulated T-box gene expression dynamics for the cell shown in (D). **(G)** Visualisation of the degree of change in tbx6 gene expression over the simulation compared to total cell movement in the direction of the anterior-posterior axis for cells starting in the posterior 25% region of the PSM. Positive Total Movement in AP represents anterior cell movement whereas negative Total Movement in AP represents posterior cell movement. Cells have the largest change in tbx6 expression when displacing anteriorly. Aberrant tbx6 expression in posterior moving cells can be observed in the bottom left quadrant where cells are moving towards the posterior yet upregulating tbx6 expression, shown by the light ochre colouring. **(H)** Visualisation of the degree of change in tbx6 gene expression over the simulation compared to total track length for cells starting in the posterior 25% region of the PSM.The total distance a cell travels shows no correlation with the degree of tbx6 gene expression change as top and bottom quadrants show similar degrees of ochre shading.

As Figure 5G and H also reveal a degree of heterogeneity in the level of tbx6 expression change within cells starting in the posterior-most 25% of the embryonic tailbud. This is reflected by the existence of patches of all three tones of orange in the top and bottom left quadrants of Figure 5G and H. In particular, the presence of light ochre patches in the bottom left quadrant of Figure 5G suggests that a subset of cells upregulate tbx6 without leaving the progenitor domain.

As a result, when simulated on live tracking data, our network predicts a degree of tbx6 expression heterogeneity within the tailbud (Figure 6A-B). To identify whether there is indeed a posterior bias of ectopic expression of *tbx6* as predicted by the live modelling, the nuclei within the PSM were segmented (Figure 6C) and then classified as either anterior or posterior relative to the posterior end of the notochord within each embryo (Figure 6D). Following this, cells with aberrant gene expression were identified in each domain, defined as expressing *tbx6* in the posterior, or *tbx16* in the anterior domain (Figure 6E). The frequency of aberrant gene expression was measured and we confirmed a posterior bias in erroneous gene expression, as predicted by the live modelling (Figure 6F) indicating that although this system is able to generate deterministic patterns at the level of the tissue (Figure 2D-F), it does so from noisy gene expression at the single cell level, as seen *in vivo* (Figure 6G).

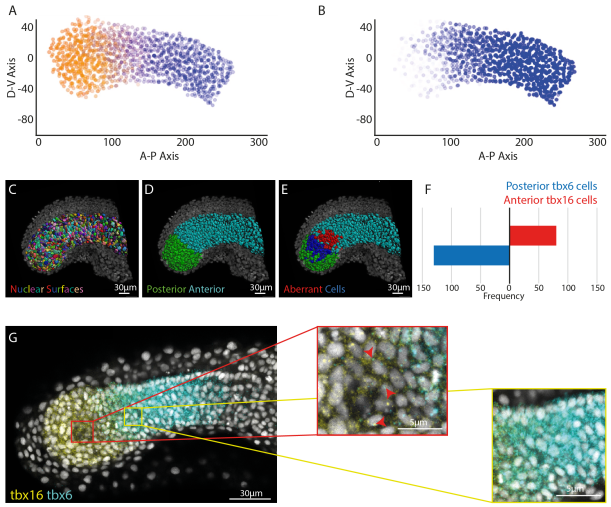

Fig. 6. Live modelling predicts cell level heterogeneity (A-B) Live modelling simulations predict that some cells upregulate tbx6 in the posterior domain of the PSM, where tbx16 would be expected to be expressed by the end of the simulation. **(A)** All three genes are shown: tbxta in red, tbx16 in yellow and tbx6 in blue. **(B)** Same as **(A)** showing only tbx6 expression in blue. **(C-E)** By examining whole mount HCR images from embryos at the 21 somite stage, and segmenting individual nuclei, cells could be classified as either posterior or anterior relative to the end of the notochord. **(F)** Cells in each of these domains could then be classified and the number of cells expressing tbx6 in the tbx16 domain and vice versa counted. This demonstrates a posterior bias in aberrant gene expression as predicted by the live modelling simulations. **(G)** These aberrant cells can be identified in slices of HCR data. **(F)** n= 3 embryos measured; bar = mean.

CONCLUSIONS

During development, cells undergo state transitions at a rate that is in part determined by cell intrinsic timers of differentiation. Mechanistically, this developmental tempo is set by the time it takes for the underlying GRN to elicit changes in gene expression. It is to a large degree also dependent on protein production and degradation rates within each cell (39; 40), and species can vary these rates in a manner that is linked to their basal metabolic rate (41). In a multi-cellular context, extrinsic signals can further tune the dynamics of this process by controlling the activation or inhibition of other nodes within a GRN, leading to the creation of a non-autonomous dynamical system where the state change of a cell

is modulated by the strengths of signal inputs that it encounters (42). Dynamical systems models appropriately account for both intrinsic and extrinsic timers of differentiation and are therefore a powerful tool to probe how gene expression patterns emerge during development (24; 25; 26; 27). Here, we present a GRN that can explain the temporal dynamics of PSM progenitor differentiation *in vitro*, and crucially is also able to recapitulate the emergence of tissue-level T-box pattern formation *in vivo* in the context of cell rearrangement.

Probing the predicted dynamics of gene expression change for single cells within our model has revealed two insights. Firstly, an unexpected degree of heterogeneity observed for tbx6 expression in the posterior progenitor domain. Gene expression heterogeneity is a common feature of progenitor populations that has in many cases been linked to underlying stochasticity in gene expression at the transcriptional level (43). While this is also likely to be the case for T-box genes in the PSM, our model points to a second source of noise in the system. GRNs are configured in such a way that produces a temporal delay in response to morphogen exposure, as such cells will not immediately adjust their expression state in situations where they move into an altered signalling environment. Dissecting these multiple sources of heterogeneity in developing systems will be an important step in fully exploring the role of gene expression noise *in vivo*.

A second insight derived from our model relates to the role of cell movements in the emergence of tissue-wide gene expression patterns. To generate patterns of T-box expression in the PSM, cells must tune their intrinsic dynamics of differentiation to the rate at which they exit the tailbud and enter the PSM. We observe that cells delayed in their exit from the progenitor region delay their upregulation of tbx6. As such, cell movements might be playing an important role in regulating the dynamics of cell differentiation, potentially by determining the level and dynamics of morphogen exposure. This emphasises the difficulty in determining gene function from mutant phenotype analysis alone as a given signal or transcription factor may have dual impact on gene expression patterns, firstly through the regulation of other network nodes to control their levels of expression but also indirectly via the regulation of cell movements within the tissue in question. This is especially important in the context of PSM development where signals such as Wnt and FGF have known functions in also regulating epithelial-to-mesenchymal transitions (7; 37; 44). In addition, tbx16 has a clear role in both the specification of mesodermal cell fate and the control of cell movement from the tailbud (38). Finally, oscillations in Wnt and FGF signalling, as well as downstream transcription factors are known to occur and offer and additional dynamic input to the system (45; 46). Here, we present a novel theoretical approach that considers both GRN interactions and cell movements. We envisage that this will be a powerful tool when testing proposed network interactions in the context of cell tracking data obtained from both wild-type and mutant embryos. In doing so, it is expected that the proposed GRN will become refined to incorporate additional feedback from both T-box gene function and cell movements to the timing of progenitor maturation. In particular, our proposed network includes a repression of tbxta by FGF, where current experimental evidence supports an activation of tbtxa (38), potentially reflecting a lack of important interactions in our current model.

The timing of progenitor contributions to the pre-somitic mesoderm are known to be controlled, at least in part, by the progressive expression of Hox genes that progressively delay progenitor addition as the body axis extends (47; 48). This timing mechanism is intrinsic to the progenitor cell populations that are fated towards the somitic mesoderm in the primitive streak, and controls the timing of cell dispersion as cells undergo an increase in cell motility (49). In this study, we follow the timing of progenitor contribution over a 3 hour time window, during which minimal changes in Hox expression occur (50). Instead, we focus on the impact that cell rearrangement has on the anterior-posterior spacing of cells across the paraxial mesoderm and how this relates to the timing of cell maturation as marked by changes in T-box gene expression. We propose that this modelling framework provides sufficient dynamic range to explore the ways that tissue morphogenesis is coordinated with cell fate. Whether this be through controlling initial gene expression heterogeneity, rates of cell movements or the dynamics of signal transduction.

Embryonic development is characterised by a series of multi-scalar interactions where dynamic state changes of individual cells, when coupled with cell movements and morphogen exposure, can lead to the emergence of gene expression patterns at the tissue level. Cell movements themselves are likely to also be impacted by tissue level properties such as the liquid-to-solid transition observed in the PSM (15; 16), and furthermore via forces acting between adjacent tissues during the process of posterior body elongation (51; 19; 52; 53). As such, it is essential that we approach the role of GRNs in development in a context of multi-tissue morphogenesis to gain a complete picture development. The live-modelling framework utilised here provides an in-road into achieving this as it enables predictions to be generated of how specific GRN topologies can lead to pattern emergence in multiple morphogenetic contexts. This might be in the context of interpreting complex mutant phenotypes or to probe how developmental systems respond to perturbations at the level of physical tissue properties, tissue geometry or multi-tissue mechanical interactions. Furthermore, while in many cases it is assumed that evolution acts to drive changes in gene expression through altering GRN interactions, our work points to an equivalent potential in altering cell movements within a tissue in question while conserving the GRNs. Exploring the multi-dimensional regulation of evolutionary change is therefore an important direction for the field.

Journal of Experimental Biology (2019) 00, jebxxxxxx. doi:10.1242/jeb.xxxxxx

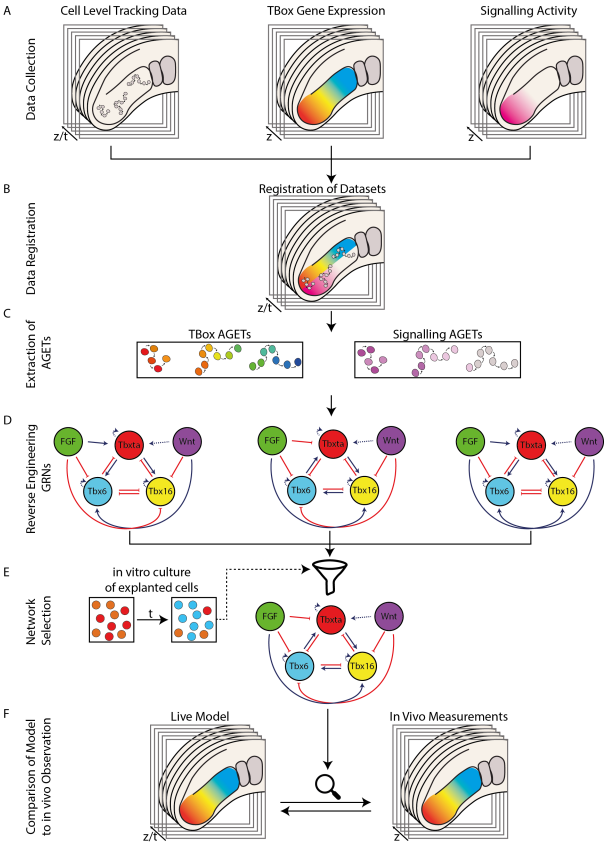

Fig. 3. Supplementary 1: Live Modelling Pipeline. **A** Three independent datasets are collected. Cell level tracking data in three dimensions is collected from live imaging individual embryos. Three dimensional T-box gene expression patterns and signalling information are obtained from fixed specimens. **B** These three datasets are registered together in 3D. **C** Individual AGETs are extracted for both signalling data and T-box gene expression. **D** Networks able to simulate these AGETs are reverse engineered using an MCMC pipeline. **E** The 100 reverse engineered networks are filtered by their ability to accurately predict gene expression patterns at the tissue level by making qualitative comparison to measured profiles (Figure 2F). Following this, networks were filtered by their ability to reproduce the observations of bimodal tbx6/tbx16 gene expression observed when cells are grown *in vitro* (Figure 4 G-I). Finally, netoworks were filtered using known network interactions obtained from the literature. **F** The remaining network is simulated on tracking data and produces patterns of T-box gene expression in 3D, which can then be compared to experimentally measured patterns.

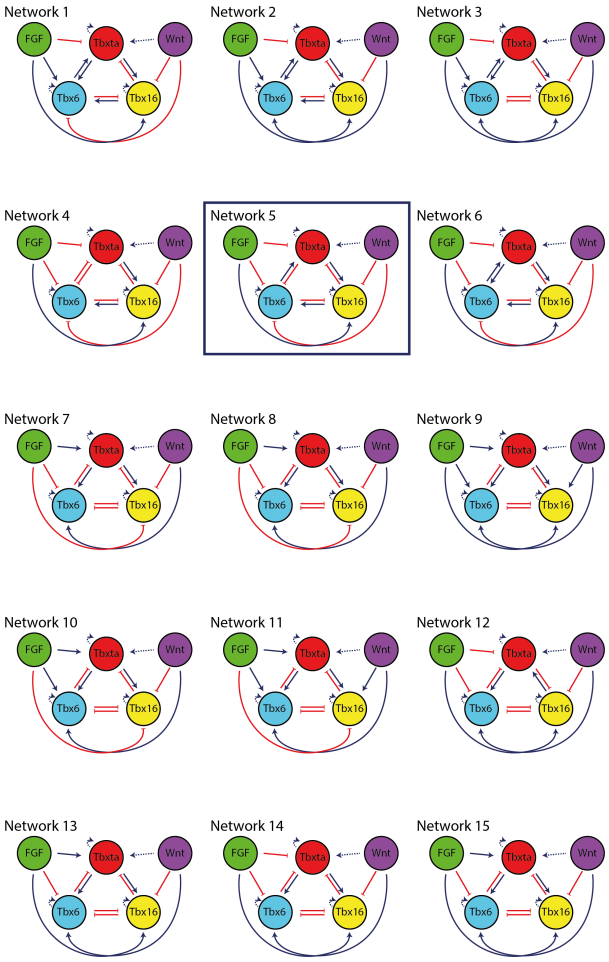

Fig. 3. Supplementary 2: 15 Possible Network Topologies. Following the generation of 100 networks which successfully able to simulate gene expression patterns of individual AGETs, filtering these networks and then clustering by network topology, 15 networks are retained. Of these, only one (Network 5) also contains the literature inferred network parameters.

MATERIALS AND METHODS

Animal Husbandry

This research was regulated under the Animals (Scientific Procedures) Act 1986 Amendment Regulations 2012 following ethical review by the University of Cambridge Animal Welfare and Ethical Review Body (AWERB). Embryos were obtained and raised in standard E3 media at 28°C. Wild Type lines are either Tüpfel Long Fin (TL), AB or AB/TL. The Tg(7xTCF-Xla.Sia:GFP) reporter line (33) was provided by the Steven Wilson laboratory. Embryos were staged as in (54).

Primary Culture of Tailbud Progenitor Cells

Cells were explanted from the tailbud as in (20; 21). Effort was made to remove the ectoderm prior to dissection. Cells were dissected in calcium and magnesium free PBS in order to promote cell dissociation. Cells were cultures in 8 well Ibidi Micro-Slides under the fully defined L15 media supplemented with PenStrep solution to limit bacterial growth.

RNA extractions were made in triplicate, from independent experiments, using Trizol Reagent (Ambion LifeTechnologies) following a standard protocol and reverse transcription using Superscript III (Invitrogen). Resultant cDNA was quantified using SYBRGreen with liquid handling robot (Qiagility, Qiagen) and analysed on a RotorGeneQ thermocycler (Qiagen).
Primer sequences:
axin2 5'-TACCCTCGGACACTTCAAGG-3'
and 5'-TGCCCTCATACATTGGCAGA-3';
sprouty4 5'-CACGCGCCCTAGTATCAAAC-3'
and 5'-GGGATCTTGGTGAAGTGTGC-3';
EF1a 5'-GGAGACTGGTGTCCTCAA-3'
and 5'-GGTGCATCTCAACAGACTT-3'.
Concentration of cDNA was estimated using an in-house MAK2 analysis method, as described previously (55).

In Situ Hybridisation Chain Reaction (HCR)

Embryos were raised to the required stage then fixed in 4% PFA in DEPC treated PBS without calcium and magnesium at 4°C overnight. Embryos were then stained using HCR following the standard zebrafish protocol found in (56). Probes, fluorescent hairpins and buffers were all purchased from Molecular Instruments. After staining, samples were counter stained with DAPI and mounted under 80% glycerol.

Immunohistochemistry

Embryos were raised to the required stage then fixed in 4% PFA in DEPC treated PBS without calcium and magnesium at 4°C overnight. Embryos were then blocked in 3% goat serum in 0.25% Triton, 1% DMSO, in PBS for one hour at room temperature. Diphosphorylated ERK was detected using the primary antibody (M9692-200UL, Sigma) diluted 1 in 500 in 3% goat serum in 0.25% Triton, 1% DMSO, in PBS. The samples were incubated at 4°C overnight then washed in 0.25% Triton, 1% DMSO, in PBS. Secondary Alexa 647nm conjugated antibodies were diluted 1 in 500 in 3% goat serum in 0.25% Triton, 1% DMSO, 1X DAPI in PBS and applied overnight at 4°C.

Imaging and Image Analysis

Samples were imaged using a Zeiss LSM700 inverted confocal microscope at 12 bit, 20X or 40X magnification, with an image resolution of 512x512 pixels. Single cell HCR was imaged using a Nikon Ti inverted widefield microscope at 63X magnification.

Image analysis of confocal images was done using the line drawing tool on Fiji (57; 58) set to a width of 50 pixels. Lines were drawn following the curve of the embryo, through the centre of the PSM from posterior PSM to the posterior most clear somite boundary. Profiles were normalised to the length of the PSM and signal intensity as individual embryos by dividing the measured value by the maximum value of that embryo.

Nuclear segmentation of whole embryos stained using HCR was conducted using a tight mask applied around the DAPI stain using Imaris (Bitplane) with a surface detail of 0.5µm. Touching surfaces were split using a seed size of 4µm. Values were exported as X, Y, Z coordinates relative to the posteriormost tip of the PSM where X, Y, Z were equal to (0, 0, 0). The PSM was then segmented by hand by deleting nuclear surfaces outside of the PSM, including notochord, spinal cord, anterior somites and ectoderm. Only the PSM closest to the imaging objective, therefore of highest imaging quality was measured with the distal PSM also removed.

Intensity mean values of each transcription factor HCR signal were exported and normalised between 0 and 1 by dividing each cell's mean signal intensity by the maximum measured within that sample, per gene. PSM length was normalised individually between 0 and 1 by division of the position in X by the maximum X value measured in each embryo.

Single cell image analysis was conducted using Imaris (Bitplane) by generating loose surface masks around the DAPI stain to capture the full nuclear region and cytoplasm. Surface masks were then filtered to remove any masks where two cells joined together or small surfaces caused by background noise, or fragmented apoptotic nuclei. The intensity sum of each channel was measured and normalised by the area of the surface, as surface area and transcript intensity had been demonstrated to correlate. Expression level was then normalised between 0 and 1 using the maximum value measured for each gene, in each experiment.

Live imaging datasets of the developing PSM was created using a TriM Scope II Upright 2-photon scanning fluorescence microscope equipped Insight DeepSee dual-line laser (tunable 710-1300 nm fixed 1040 nm line). Embryo was imaged with a 25X 1.05 NA water dipping objective. Time step and frame number as per figure legend. Embryos laterally in low melting agarose with the entire tail cut free to permit normal development (59).

Model formulation

We formulated the T-box gene regulatory network using a dynamical systems formulation. The models aim is to recapitulate the dynamics of T-box gene expression for any cell, or rather a general cell, in the developing zebrafish PSM. We use a connectionist model formulation previously used to model other developmental patterning processes (60).

The mRNA concentrations encoded by the T-box genes *tbxta*, *tbx16* and *tbx6* are represented by the state variables of the dynamical system. For each gene, the concentration of its associated mRNA a at time t is given by $g^a(t)$. mRNA concentration over time is governed by the following system of three coupled ordinary differential equations:

$$\frac{dg_a(t)}{dt} = R_a\phi(u_a) - \lambda_a g_a(t) \quad (1)$$

where R^a and λ^a respectively represent the rates of mRNA production and decay. ϕ is a sigmoid regulation-expression function used to represent the cooperative, saturating, coarse-grained kinetics of transcriptional regulation and introduces non-linearities into the model that enable it to exhibit complex behaviours:

$$\phi(u_a) = \frac{1}{2}\left(\frac{u_a}{\sqrt{(u_a)^2+1}} + 1\right), \quad (2)$$

where

$$u_a = \sum_{b\in G} W^{ba} g_b(t) + \sum_{s\in S} E^{sa} g_s(t) + h_a. \quad (3)$$

$G = \{tbxta, tbx16, tbx6\}$ is the set of T-box genes while $S = \{\mathrm{Wnt}, \mathrm{FGF}\}$ is the set of external regulatory inputs provided by the Wnt and FGF signalling environments. The concentrations of the external regulators g_s are interpolated from quantified spatial mRNA expression data (Figure 1J) and translated into time as explained in the main text to used as dynamic inputs to the model. Changing Wnt and FGF concentrations over time renders the parameter term $\sum_{s\in S} E^{sa} g_s(t)$ time-dependent and therefore the model non-autonomous (61; 25).

The interconnectivity matrices W and E house the parameters representing the regulatory interactions among the T-box genes, and from Wnt and FGF to the T-box genes, respectively. Matrix elements w^{ba} and e^{sa} are the parameters representing the effect of regulator b or s on target gene a. These can be positive (representing an activation from b or s onto a), negative (repression), or close to zero (no interaction). h_a is a threshold parameter representing the basal activity of gene a, which acknowledges the presence of regulators absent from our model. Model parameters are detailed in Table S1.

Model fitting and selection

We have developed a methodology that makes it possible to reverse-engineer gene regulatory networks that might be driving 4D tissue-level pattern formation during morphogenesis. Prior to the development of this methodology, it was only possible to confidently reverse-engineer GRNs underlying pattern formation in developmental processes where the timescales of pattern formation and morphogenesis could be separated. This was because it is only possibly to accurately quantify the gene expression dynamics of multiple genes of interest in a single cell (or at a given position in the tissue) from static confocal stains of the tissue at different developmental stages if the cells are not significantly changing their position over time. Otherwise, the quantification at a given position in the tissue reflects the gene expression dynamics of many cells, and not that of a single cell, which is what the GRN is modelling, leading to inaccurate GRN predictions. This limitation has hence historically greatly restricted the types of patterning processes that could be reverse-engineered.

In order to extend the application of reverse-engineering approaches to a wider variety of patterning processes -particularly those where the timescales of pattern formation and morphogenesis are coupled - we have developed a novel methodology that is based on approximating gene expression trajectories of single cell tracks and using these for gene regulatory network inference. In brief, this methodology can be split into two main parts: generating approximated gene expression trajectories (AGETs) for every cell track, and using a Markov Chain Monte Carlo parameter sampling algorithm to infer candidate GRNs that can recapitulate the gene expression dynamics of a subset of the AGETs. Candidate GRNs are then selected for further study based on their ability to recapitulate the tissue-level patterning dynamics, and other case-specific factors.

In order to construct the AGETs we align and project gene and signalling quantifications obtained from confocal imaging HCR and immuno stained tailbuds onto each time frame in the time-lapse of the developing PSM. Each cell in the time frame is assigned gene expression and signalling levels averaged from the five closest cells to it from the quantification. This is repeated for each frame, and results in an approximated gene and signalling trajectory for each cell in the movie. Ten AGETs were then selected pseudo-randomly along the PSM and used for network inference. The MCMC algorithm was run 100 times, and solutions were resolved into 22 clusters that were able to recapitulate tissue-level T-box patterning when simulated on the tracks. Representative networks of these 22 clusters were then used to simulate the dissociation experiments and one network was selected for further study. For further details of this methodology please refer to the methodology paper (8).

Live modelling framework.

The live-modelling framework consists on simulating gene regulatory networks in every cell represented in tracks obtained from live-imaging a developing tissue, using as initial conditions approximated concentrations of *tbxta*, *tbx16* and *tbx6* in each cell, and updating Wnt and FGF values dynamically as the cells' positions changes during morphogenesis. The cell tracks used in this work, span four somite stages and were obtained from live-imaging a developing zebrafish PSM using a multiphoton microscope. The position of each cell in the PSM was recorded in 3D space as an (x, y, z) coordinate every 2.5 minutes. The coordinate system was such that the origin (0,0,0) was set at the posterior-most tip of the PSM. The positive x-axis runs in the posterior to anterior direction through the middle of the PSM, the positive y-axis runs from centre to dorsal PSM and the positive z-axis, from centre to lateral PSM. The raw tracking data were manually modified to terminate tracks once these had entered a newly formed somite, ensuring that the dataset would only contain the tracks of cells within the PSM. Newly formed somites can be identified in the tracks by eye as soon as their posterior boundary forms.

The simulations are initialised using T-box gene expression and signalling profiles (Figure 1C, J) that were used to fit the gene regulatory network model. At the first time point, T-box expression profiles (Figure 1C) are projected onto the normalised length of the PSM, and cells are assigned *tbxta*, *tbx16* and *tbx6* values according to their posterior to anterior position (x-axis). These values will be used as the initial conditions from which to simulate the gene regulatory network model in every cell. The same methodology is used to assign each cell with initial Wnt and FGF values.

The model is allowed to run in every cell for the duration between time points in the tracks using the Wnt and FGF values previously assigned. At the next time point, the position of the cell is updated to the tracking data. The new length of the PSM is again normalised, signalling profiles are the projected onto the newly normalised PSM and cells will update their Wnt and FGF values again according to their new relative positions in the PSM. The model will run again simulating the time between tracking time

points using the last simulated *tbxta*, *tbx16* and *tbx6* values as the initial conditions and the recently updated values for Wnt and FGF. This will be done iteratively until the last tracking time point. Cells which appear between time points, following cell division or a new track for example, are initialised in the same way cells were at the first time point. By simulating a GRNs in each cell of a developing tissue, we are able to asses it's patterning capabilities within a realistic morphogenetic context, including realistic accounts of tissue shape changes and cellular rearrangements.

Acknowledgements

We would like to thank Buzz Baum, Laurel Rohde, Andrew Oates and the team, Dillan Saunders and Meagan Hennessy for feedback on this manuscript. Shannon Taylor provided significant insights to improve the manuscript at the revision stage. We would like to thank the Steven Wilson lab for sharing the Tg(7xTCF-Xla.Sia:GFP) line, and Kawamura Akinori for the Tbx6::GFP line. Thanks to the Cambridge Advanced Imaging Centre (CAIC) for imaging support.

Competing interests

None

Contribution

Insert the Contribution text here.

Funding

K.S. was initially supported by Wave 1 of the UKRI Strategic Priorites Fund under the EPSRC grant EP/T001569/1, particularly the "AI for Science and Government" theme within that grant and the Alan Turing Institute, and later by a by a Henry Dale Fellowship granted to B.S. jointly funded by the Wellcome Trust and the Royal Society (109408/Z/15/Z). T.F., S.H. and B.S. are supported by a Henry Dale Fellowship jointly funded by the Wellcome Trust and the Royal Society (109408/Z/15/Z) and T.F. by a scholarship from the Cambridge Trust, University of Cambridge. L.T. is supported by a scholarship from the BBSRC. Y.W. is supported by a summer vacation stipend from St Catharine's College, University of Cambridge. B.C. is supported by a Stipend from the Bedford Fund, King's College, University of Cambridge and a scholarship from the Wellcome Trust. B.V. was supported by a Herschel Smith Postdoctoral Fellowship, University of Cambridge, and Department of Biology at University of Oxford and Jesus College, University of Oxford. B. C. is supported by a Wellcome Trust Developmental Mechanisms PhD studentship (222279/Z/20/Z).

Data availability

Insert the Data availability text here.

Supplementary

Insert the supplementary text text here.

REFERENCES

[1]Henrique D, Abranches E, Verrier L, Storey KG. Neuromesodermal progenitors and the making of the spinal cord. Development. 2015;142(17):2864-75.

[2]Wilson V, Olivera-Martinez I, Storey KG. Stem cells, signals and vertebrate body axis extension. Development. 2009 5;136(10):1591-604.

[3]Gomez C, Özbudak EM, Wunderlich J, Baumann D, Lewis J, Pourquié O. Control of segment number in vertebrate embryos. Nature. 2008;454(7202):335-9.

[4]Martin BL. Factors that coordinate mesoderm specification from neuromesodermal progenitors with segmentation during vertebrate axial extension. Seminars in Cell and Developmental Biology. 2016 1;49:59-67. Available from: https://www.sciencedirect.com/science/article/pii/S1084952115300124.

[5]Warga RM, Mueller RL, Ho RK, Kane DA. Zebrafish Tbx16 regulates intermediate mesoderm cell fate by attenuating Fgf activity. Developmental Biology. 2013 11;383(1):75-89.

[6]Nikaido M, Kawakami A, Sawada A, Furutani-Seiki M, Takeda H, Araki K. Tbx24, encoding a T-box protein, is mutated in the zebrafish somite-segmentation mutant fused somites. Nature genetics. 2002;31(2):195-9.

[7]Bajard L, Morelli LG, Ares S, Pécréaux J, Jülicher F, Oates AC. Wnt-regulated dynamics of positional information in zebrafish somitogenesis. Development. 2014;141(6):1381-91.

[8]Spiess K, Fulton T, Thomson L, Hwang S, Toh K, Saunders D, et al. Approximated gene expression trajectories (AGETs) for gene regulatory network inference on cell tracks. bioRxiv. 2022.

[9]Palmeirim I, Henrique D, Ish-Horowicz D, Pourquié O. Avian hairy gene expression identifies a molecular clock linked to vertebrate segmentation and somitogenesis. Cell. 1997;91(5):639-48.

[10]Dubrulle J, McGrew MJ, Pourquié O. FGF signaling controls somite boundary position and regulates segmentation clock control of spatiotemporal Hox gene activation. Cell. 2001 7;106(2):219-32.
[11]Aulehla A, Pourquié O. Oscillating signaling pathways during embryonic development. Current Opinion in Cell Biology. 2008 12;20(6):632-7.
[12]Aulehla A, Wehrle C, Brand-Saberi B, Kemler R, Gossler A, Kanzler B, et al. Wnt3a plays a major role in the segmentation clock controlling somitogenesis. Developmental Cell. 2003 3;4(3):395-406.
[13]Bénazéraf B, Francois P, Baker RE, Denans N, Little CD, Pourquié O. A random cell motility gradient downstream of FGF controls elongation of an amniote embryo. Nature. 2010;466(7303):248-52.
[14]Xiong F, Ma W, Bénazéraf B, Mahadevan L, Pourquié O. Mechanical coupling coordinates the co-elongation of axial and paraxial tissues in avian embryos. Developmental Cell. 2020;55(3):354-66.
[15]Mongera A, Rowghanian P, Gustafson HJ, Shelton E, Kealhofer DA, Carn EK, et al. A fluid-to-solid jamming transition underlies vertebrate body axis elongation. Nature. 2018 9;561(7723):1.
[16]Serwane F, Mongera A, Rowghanian P, Kealhofer DA, Lucio AA, Hockenbery ZM, et al. In vivo quantification of spatially varying mechanical properties in developing tissues. Nature methods. 2017;14(2):181-6.
[17]Lawton AK, Nandi A, Stulberg MJ, Dray N, Sneddon MW, Pontius W, et al. Regulated tissue fluidity steers zebrafish body elongation. Development (Cambridge). 2013 2;140(3):573-82.
[18]Das D, Jülich D, Schwendinger-Schreck J, Guillon E, Lawton AK, Dray N, et al. Organization of embryonic morphogenesis via mechanical information. Developmental cell. 2019;49(6):829-39.
[19]Thomson L, Muresan L, Steventon B. The zebrafish presomitic mesoderm elongates through compaction-extension. Cells & Development. 2021.
[20]Webb AB, Lengyel IM, Jörg DJ, Valentin G, Jülicher F, Morelli LG, et al. Persistence, period and precision of autonomous cellular oscillators from the zebrafish segmentation clock. eLife. 2016 2;5:e08438.
[21]Rohde LA, Bercowsky-Rama A, Negrete J, Valentin G, Naganathan SR, Desai RA, et al. Cell-autonomous generation of the wave pattern within the vertebrate segmentation clock. bioRxiv. 2021.
[22]Yasuhiko Y, Haraguchi S, Kitajima S, Takahashi Y, Kanno J, Saga Y. Tbx6-mediated Notch signaling controls somite-specific Mesp2 expression. Proceedings of the National Academy of Sciences. 2006;103(10):3651-6.
[23]Jaeger J, Monk N. Bioattractors: dynamical systems theory and the evolution of regulatory processes. The Journal of physiology. 2014;592(11):2267-81.
[24]Crombach A, Wotton KR, Jiménez-Guri E, Jaeger J. Gap gene regulatory dynamics evolve along a genotype network. Molecular biology and evolution. 2016;33(5):1293-307.
[25]Verd B, Crombach A, Jaeger J. Classification of transient behaviours in a time-dependent toggle switch model. BMC systems biology. 2014;8(1):1-19.
[26]Sagner A, Briscoe J. Morphogen interpretation: concentration, time, competence, and signaling dynamics. Wiley Interdisciplinary Reviews: Developmental Biology. 2017;6(4):e271.
[27]Kicheva A, Bollenbach T, Ribeiro A, Valle HP, Lovell-Badge R, Episkopou V, et al. Coordination of progenitor specification and growth in mouse and chick spinal cord. Science. 2014;345(6204).
[28]Row RH, Tsotras SR, Goto H, Martin BL. The zebrafish tailbud contains two independent populations of midline progenitor cells that maintain long-term germ layer plasticity and differentiate in response to local signaling cues. Development. 2016 01;143(2):244-54. Available from: https://doi.org/10.1242/dev.129015.
[29]Ban H, Yokota D, Otosaka S, Kikuchi M, Kinoshita H, Fujino Y, et al. Transcriptional autoregulation of zebrafish *tbx6* is required for somite segmentation. Development. 2019 8:dev.177063.
[30]Balaskas N, Ribeiro A, Panovska J, Dessaud E, Sasai N, Page KM, et al. Gene regulatory logic for reading the Sonic Hedgehog signaling gradient in the vertebrate neural tube. Cell. 2012;148(1-2):273-84.
[31]Raspopovic J, Marcon L, Russo L, Sharpe J. Digit patterning is controlled by a Bmp-Sox9-Wnt Turing network modulated by morphogen gradients. Science. 2014;345(6196):566-70.
[32]Verd B, Clark E, Wotton KR, Janssens H, Jiménez-Guri E, Crombach A, et al. A damped oscillator imposes temporal order on posterior gap gene expression in Drosophila. PLoS biology. 2018;16(2):e2003174.
[33]Moro E, Ozhan-Kizil G, Mongera A, Beis D, Wierzbicki C, Young RM, et al. In vivo Wnt signaling tracing through a transgenic biosensor fish reveals novel activity domains. Developmental Biology. 2012 6;366(2):327-40.
[34]Kawamura A, Koshida S, Hijikata H, Ohbayashi A, Kondoh H, Takada S. Groucho-associated transcriptional repressor ripply1 is required for proper transition from the presomitic mesoderm to somites. Developmental Cell. 2005 12;9(6):735-44.
[35]Bouldin CM, Manning AJ, Peng YH, Farr GH, Hung KL, Dong A, et al. Wnt signaling and tbx16 form a bistable switch to commit bipotential progenitors to mesoderm. Development. 2015;142(14):2499-507.
[36]Fior R, Maxwell AA, Ma TP, Vezzaro A, Moens CB, Amacher SL, et al. The differentiation and movement of presomitic mesoderm progenitor cells are controlled by Mesogenin 1. Development (Cambridge, England). 2012 7;129(14):3311-23.
[37]Goto H, Kimmey SC, Row RH, Matus DQ, Martin BL. FGF and canonical Wnt signaling cooperate to induce paraxial mesoderm from tailbud neuromesodermal progenitors through regulation of a two-step epithelial to mesenchymal transition. Development. 2017;144(8):1412-24.
[38]Griffin K, Amacher S, Kimmel C, Kimelman D. Molecular identification of spadetail: regulation of zebrafish trunk and tail mesoderm formation by T-box genes. Development. 1998 9;122(12):4119-29.
[39]Matsuda M, Hayashi H, Garcia-Ojalvo J, Yoshioka-Kobayashi K, Kageyama R, Yamanaka Y, et al. Species-specific segmentation clock periods are due to differential biochemical reaction speeds. Science (New York, NY). 2020 9;369(6510). Available from: https://pubmed.ncbi.nlm.nih.gov/32943519/.
[40]Rayon T, Stamataki D, Perez-Carrasco R, Garcia-Perez L, Barrington C, Melchionda M, et al. Species-specific pace of development is associated with differences in protein stability. Science. 2020 9;369(6509). Available from: https://www.science.org/doi/abs/10.1126/science.aba7667.
[41]Diaz-Cuadros M, Miettinen TP, Sheedy D, Díaz-García CM, Gapon S, Hubaud A, et al. Metabolic regulation of species-specific developmental rates. bioRxiv. 2021 8:2021.08.27.457974. Available from: https://www.biorxiv.org/content/10.1101/2021.08.27.457974v1https://www.biorxiv.org/content/10.1101/2021.08.27.457974v1.abstract.
[42]Busby L, Steventon B. Tissue Tectonics and the Multi-Scale Regulation of Developmental Timing. Preprints. 2020 jun.
[43]Moris N, Pina C, Arias AM. Transition states and cell fate decisions in epigenetic landscapes. Nature Reviews Genetics. 2016. Available from: http://www.nature.com/doifinder/10.1038/nrg.2016.98.
[44]Row RH, Maître JL, Martin BL, Stockinger P, Heisenberg CP, Kimelman D. Completion of the epithelial to mesenchymal transition in zebrafish mesoderm requires Spadetail. Developmental Biology. 2011 6;354(1):102-10.
[45]Krol AJ, Roellig D, Dequéant ML, Tassy O, Glynn E, Hattem G, et al. Evolutionary plasticity of segmentation clock networks. Development. 2011 07;138(13):2783-92. Available from: https://doi.org/10.1242/dev.063834.
[46]Simsek MF, Chandel AS, Saparov D, Zinani OQ, Clason N, Özbudak EM. Periodic inhibition of Erk activity drives sequential somite segmentation. Nature. 2023;613(7942):153-9.
[47]Moreau C, Caldarelli P, Rocancourt D, Roussel J, Denans N, Pourquie O, et al. Timed Collinear Activation of Hox Genes during Gastrulation Controls the Avian Forelimb Position. Current Biology. 2019 Jan;29(1):35-50.e4. Available from: https://doi.org/10.1016/j.cub.2018.11.009.
[48]Denans N, Iimura T, Pourquié O. Hox genes control vertebrate body elongation by collinear Wnt repression. eLife. 2015 feb;4:e04379. Available from: https://doi.org/10.7554/eLife.04379.
[49]Busby L, Nájera GS, Steventon B. A population intrinsic timer controls Hox gene expression and cell dispersion during progenitor addition to the body axis. bioRxiv. 2023. Available from: https://www.biorxiv.org/content/early/2023/05/10/2023.05.10.540133.
[50]Prince VE, Joly L, Ekker M, Ho RK. Zebrafish hox genes: genomic organization and modified colinear expression patterns in the trunk. Development.

1998 02;125(3):407-20. Available from: https://doi.org/10.1242/dev.125.3.407.

[51]McLaren SBP, Steventon BJ. Anterior expansion and posterior addition to the notochord mechanically coordinate zebrafish embryo axis elongation. Development. 2021 9;148(18).

[52]Steventon B, Duarte F, Lagadec R, Mazan S, Nicolas JF, Hirsinger E. Species-specific contribution of volumetric growth and tissue convergence to posterior body elongation in vertebrates. Development (Cambridge, England). 2016 5;143(10):1732-41. Available from: http://www.ncbi.nlm.nih.gov/pubmed/26989170.

[53]Tlili S, Yin J, Rupprecht JF, Mendieta-Serrano MA, Weissbart G, Verma N, et al. Shaping the zebrafish myotome by intertissue friction and active stress. Proceedings of the National Academy of Sciences of the United States of America. 2019 12;116(51):25430-9. Available from: https://www.pnas.org/content/116/51/25430https://www.pnas.org/content/116/51/25430.abstract.

[54]Kimmel CB, Ballard WW, Kimmel SR, Ullmann B, Schilling TF. Stages of embryonic development of the zebrafish. Developmental Dynamics. 1995 1;203(3):253-310.

[55]Turner Da, Hayward PC, Baillie-Johnson P, Rué P, Broome R, Faunes F, et al. Wnt/ -catenin and FGF signalling direct the specification and maintenance of a neuromesodermal axial progenitor in ensembles of mouse embryonic stem cells. Development. 2014 nov;141(22):4243-53. Available from: http://dev.biologists.org/cgi/doi/10.1242/dev.112979.

[56]Choi HMT, Schwarzkopf M, Fornace ME, Acharya A, Artavanis G, Stegmaier J, et al. Third-generation in situ hybridization chain reaction: Multiplexed, quantitative, sensitive, versatile, robust. Development (Cambridge). 2018 6;145(12).

[57]Schindelin J, Arganda-Carreras I, Frise E, Kaynig V, Longair M, Pietzsch T, et al. Fiji: An open-source platform for biological-image analysis. Nature Methods. 2012 7;9(7):676-82.

[58]Schneider Ca, Rasband WS, Eliceiri KW. NIH Image to ImageJ: 25 years of image analysis. Nature Methods. 2012;9(7):671-5.

[59]Hirsinger E, Steventon B. A versatile mounting method for long term imaging of zebrafish development. Journal of Visualized Experiments. 2017 jan;2017(119):e55210. Available from: https://www.jove.com/v/55210/a-versatile-mounting-method-for-long-term-imaging-zebrafish.

[60]Mjolsness E, Sharp DH, Reinitz J. A connectionist model of development. Journal of theoretical Biology. 1991;152(4):429-53.

[61]Collier JR, Monk NA, Maini PK, Lewis JH. Pattern formation by lateral inhibition with feedback: a mathematical model of delta-notch intercellular signalling. Journal of theoretical Biology. 1996;183(4):429-46.

[62]Briscoe J, Small S. Morphogen rules: design principles of gradient-mediated embryo patterning. Development. 2015;142(23):3996-4009.

[63]Venzin OF, Oates AC. What are you synching about? Emerging complexity of Notch signaling in the segmentation clock. Developmental biology. 2020;460(1):40-54.

[64]Strogatz SH. Nonlinear dynamics and chaos with student solutions manual: With applications to physics, biology, chemistry, and engineering. CRC press; 2018.

[65]Martin BL, Kimelman D. Regulation of canonical Wnt signaling by Brachyury is essential for posterior mesoderm formation. Developmental cell. 2008;15(1):121-33.

[66]Nüsslein-volhard C, Wieschaus E. Mutations affecting segment number and polarity in drosophila. Nature. 1980;287(5785):795-801.

[67]Zagorski M, Tabata Y, Brandenberg N, Lutolf MP, Bollenbach T, Briscoe J, et al. Decoding of position in the developing neural tube from antiparallel morphogen gradients. Science. 2017;356:1379-83.

[68]Verd B, Crombach A, Jaeger J. Dynamic Maternal Gradients Control Timing and Shift-Rates for Drosophila Gap Gene Expression. PLOS Computational Biology. 2017 2;13(2):e1005285.

[69]Martinez Arias A, Steventon B. On the nature and function of organizers. Development (Cambridge). 2018 3;145(5).

[70]Pourquié O. Vertebrate Somitogenesis. Annual Review of Cell and Developmental Biology. 2001 11;17(1):311-50.

[71]Mallo M. Revisiting the involvement of signaling gradients in somitogenesis. The FEBS Journal. 2016 4;283(8):1430-7.

[72]Steventon B, Duarte F, Lagadec R, Mazan S, Nicolas JF, Hirsinger E. Species-specific contribution of volumetric growth and tissue convergence to posterior body elongation in vertebrates. Development (Cambridge, England). 2016 5;143(10):1732-41.

[73]Attardi A, Fulton T, Florescu M, Shah G, Muresan L, Lenz MO, et al. Neuromesodermal progenitors are a conserved source of spinal cord with divergent growth dynamics. Development. 2018 10:dev.166728.

[74]McMillen P, Holley SA. The tissue mechanics of vertebrate body elongation and segmentation. Current Opinion in Genetics and Development. 2015;32:106-11.

[75]Goldbeter A, Pourquié O. Modeling the segmentation clock as a network of coupled oscillations in the Notch, Wnt and FGF signaling pathways. Journal of Theoretical Biology. 2008 6;252(3):574-85.

[76]Holley SA, Takeda H. Catching a wave: the oscillator and wavefront that create the zebrafish somite. Seminars in Cell & Developmental Biology. 2002 12;13(6):481-8.

[77]Aulehla A, Pourquié O. Signaling gradients during paraxial mesoderm development. Cold Spring Harbor perspectives in biology. 2010 2;2(2):a000869.

[78]Bénazéraf B, Francois P, Baker RE, Denans N, Little CD, Pourquié O. A random cell motility gradient downstream of FGF controls elongation of an amniote embryo. Nature. 2010 7;466(7303):248-52.

[79]Kimelman D. Tales of Tails (and Trunks). Forming the Posterior Body in Vertebrate Embryos. vol. 116. 1st ed. Elsevier Inc.; 2016.

[80]Manning AJ, Kimelman D. Tbx16 and Msgn1 are required to establish directional cell migration of zebrafish mesodermal progenitors. Developmental Biology. 2015 10;406(2):172-85.

[81]Petrungaro G, Morelli LG, Uriu K. Information flow in the presence of cell mixing and signaling delays during embryonic development. Seminars in Cell and Developmental Biology. 2018;93:26-35. Available from: https://www.sciencedirect.com/science/article/pii/S108495211730561X?via%3Dihub.

[82]Uriu K, Ares S, Oates AC, Morelli LG. Optimal cellular mobility for synchronization arising from the gradual recovery of intercellular interactions. Physical Biology. 2012 6;9(3).

[83]Uriu K, Morelli LG. Collective cell movement promotes synchronization of coupled genetic oscillators. Biophysical Journal. 2014 7;107(2):514-26.

[84]Uriu K, Morelli LG, Oates AC. Interplay between intercellular signaling and cell movement in development. Seminars in Cell and Developmental Biology. 2014 11;35:66-72.

[85]Ridelis I, Schmidt A, Teichmann A, Furkert J, Wiesner B, Schülein R. Use of Kikume green–red fusions to study the influence of pharmacological chaperones on trafficking of G protein-coupled receptors. FEBS Letters. 2012 3;586(6):784-91.

[86]Tsutsui H, Karasawa S, Shimizu H, Nukina N, Miyawaki A. Semi-rational engineering of a coral fluorescent protein into an efficient highlighter. EMBO reports. 2005 3;6(3):233-8.

[87]Habuchi S, Tsutsui H, Kochaniak AB, Miyawaki A, van Oijen AM. mKikGR, a Monomeric Photoswitchable Fluorescent Protein. PLoS ONE. 2008 12;3(12):e3944.

[88]Schröter C, Herrgen L, Cardona A, Brouhard GJ, Feldman B, Oates AC. Dynamics of zebrafish somitogenesis. Developmental Dynamics. 2008 3;237(3):545-53.

[89]Delfini MC, Dubrulle J, Malapert P, Chal J, Pourquié O. Control of the segmentation process by graded MAPK/ERK activation in the chick embryo. Proceedings of the National Academy of Sciences of the United States of America. 2005 8;102(32):11343-8.

[90]Simone DA, Evanitsky MN, Hayden L, Cox BD, Wang J, Tornini VA, et al. Control of osteoblast regeneration by a train of Erk activity waves. Nature. 2021 1:1-5.

[91]De Simone A, Evanitsky MN, Hayden L, Cox BD, Wang J, Tornini VA, et al. Control of osteoblast regeneration by a train of Erk activity waves. Nature. 2021 jan;590(7844):129. Available from: https://doi.org/10.1038/s41586-020-03085-8.